Time-Diverse Doppler-Only LEO PNT: Initial Solution

Megan O. Moore, Mark L. Psiaki, R. Michael Buehrer *Virginia Tech*

BIOGRAPHY

Megan O. Moore is currently a PhD student at Virginia Tech in the Electrical and Computer Engineering department. She graduated with her MS in EE from the same in 2021. Her area of research includes alternative PNT technologies and PNT resiliency. Her 2023 MILCOM paper "Time Diverse Doppler Only LEO for PNT" won the Bose best paper award.

Mark L. Psiaki is Professor and Kevin T. Crofton Faculty Chair of Aerospace and Ocean Engineering at Virginia Tech. He is also Professor Emeritus of Mechanical and Aerospace Engineering at Cornell University. He holds a Ph.D. in Mechanical and Aerospace Engineering from Princeton University. He is a Fellow of both the ION and the AIAA, and he received the ION Satellite Division's Kepler award. His research interests are in the areas of navigation, spacecraft attitude and orbit determination, remote sensing, and general methods for estimation, filtering, and detection.

R. Michael Buehrer (IEEE Fellow 2016) joined Virginia Tech from Bell Labs in 2001. He is currently a Professor of Electrical Engineering and the former Director of Wireless @ Virginia Tech, a comprehensive research group focusing on wireless communications, radar and localization. Dr. Buehrer was named an IEEE Fellow in 2016 "for contributions to wideband signal processing in communications and geolocation." His current research interests include geolocation, machine learning for wireless communications and radar, position location networks, electronic warfare, dynamic spectrum sharing, Multiple Input Multiple Output (MIMO) communications, spread spectrum, interference mitigation, and propagation modeling.

ABSTRACT

This paper develops Doppler-based Geometric Dilution of Precision (D-GDOP) analysis for time-diverse Doppler-only positioning and presents an associated batch filter. The former Doppler-only positioning solution requires at least eight satellites to be view simultaneously and discards previous Doppler measurements. In cases where fewer than eight satellites are available, using Doppler measurements from multiple points in time allows a complete solution to be determined. In cases where eight or more are available, using additional time-samples can further reduce D-GDOP and improve positioning accuracy. This work presents an initial batch filter solution that assumes constant velocity and constant clock-offset rate. By considering an additional 10 seconds of previous measurements, position and clock-offset errors were cut in half. However, because these assumptions are unrealistic for significant time spans this work also presents and tests an initial time-varying Kalman filter model and defines a D-GDOP metric for it.

I. INTRODUCTION

Global Navigation Satellite Systems (GNSS) are a critical part of our infrastructure; the positioning, navigation, and timing (PNT) information they provide are essential to numerous critical industries Furchtgott-Roth (2022). Despite their critical nature, they have been shown to be vulnerable to various attacks Dovis (2015). The high cost of fielding satellites at medium-Earth orbit (MEO) makes it a difficult – and expensive – prospect to upgrade them in response to emerging threats. This has led to increased interest in leveraging existing signals of opportunity (SOP) for PNT. In particular, SOPs from large communication constellations at low-Earth orbit (LEO) like Starlink and OneWeb have made Doppler-only positioning a viable alternative. Psiaki (2021) introduces a full Doppler-only positioning solution that simultaneously solves for user-position and user-velocity. To solve for these terms – along with an additional two terms for receiver clock-offset and clock-offset rate – eight satellites are required to be in view.

Moore et al. (2023) demonstrated that eight satellites were unlikely to be consistently in view for either OneWeb or Starlink. The work assumed elevation masks of 25° and 40° and propagated orbits based on data from May, 2023. Note that the higher elevation masks account for the increased directivity of the communication satellites' transmissions. With the Starlink constellation continually growing, eight satellites might now be consistently in view – however, the thin, spot beams Starlink uses and Starlink's connectivity policy make it more likely that only up to four signals will be received from any single user at a time FCC (2018). Figure 1 shows the visibility of OneWeb satellites from Cape Canaveral, FL over approximately one orbital period assuming an elevation mask of 25°. The horizontal axis plots time. The left-hand vertical axis shows the OneWeb satellite identifier numbers of the corresponding plotted blue dots. The right-hand vertical axis shows the number of visible satellites of the plotted red circles. While the average number of satellites in view was over eight, there were quite a few cases where only six or seven satellites are in view. In those cases, the batch point solution presented in Psiaki (2021) could not be

Preprint from ION GNSS+ 2024

calculated. Kassas et al. (2023) has proposed addressing this limitation by using signals from multiple constellations in order to see signals from at least eight satellites simultaneously. Such an approach comes at the expense of a more complicated receiver.

Moore et al. (2023) proposed that, rather than requiring eight satellites to be in view simultaneously, it should be possible to operate with fewer satellites by taking multiple measurements of each available satellite over multiple time samples. The OneWeb satellites in Figure 1 stayed in view for an average of 375 seconds with a maximum of 540 and a minimum of just 60 seconds. Figure 2 shows an example case with seven OneWeb satellites in view at 8:46 pm and their projected trajectory over the next 100 seconds. In just 100 seconds, the satellites move appreciably and give rise to significant spatial diversity. The Doppler based geometric dilution of precision (D-GDOP) calculations used in Moore et al. (2023) were based on the model defined in Psiaki (2021) and McLemore and Psiaki (2021). Unfortunately, that analysis made inconsistent assumptions. It assumed that the velocity was a constant, and potentially non-zero, but it also assumed position was constant. Similarly, it also assumed that the clock-offset rate was a constant, and potentially non-zero, but is that the clock-offset was a constant.

This paper presents a physically consistent D-GDOP analysis and an initial point solution for time-diverse Doppler-only positioning assuming constant user velocity and constant clock offset. Additionally, the paper defines a method of D-GDOP analysis for a time-varying Kalman filter for modeling more realistic scenarios.

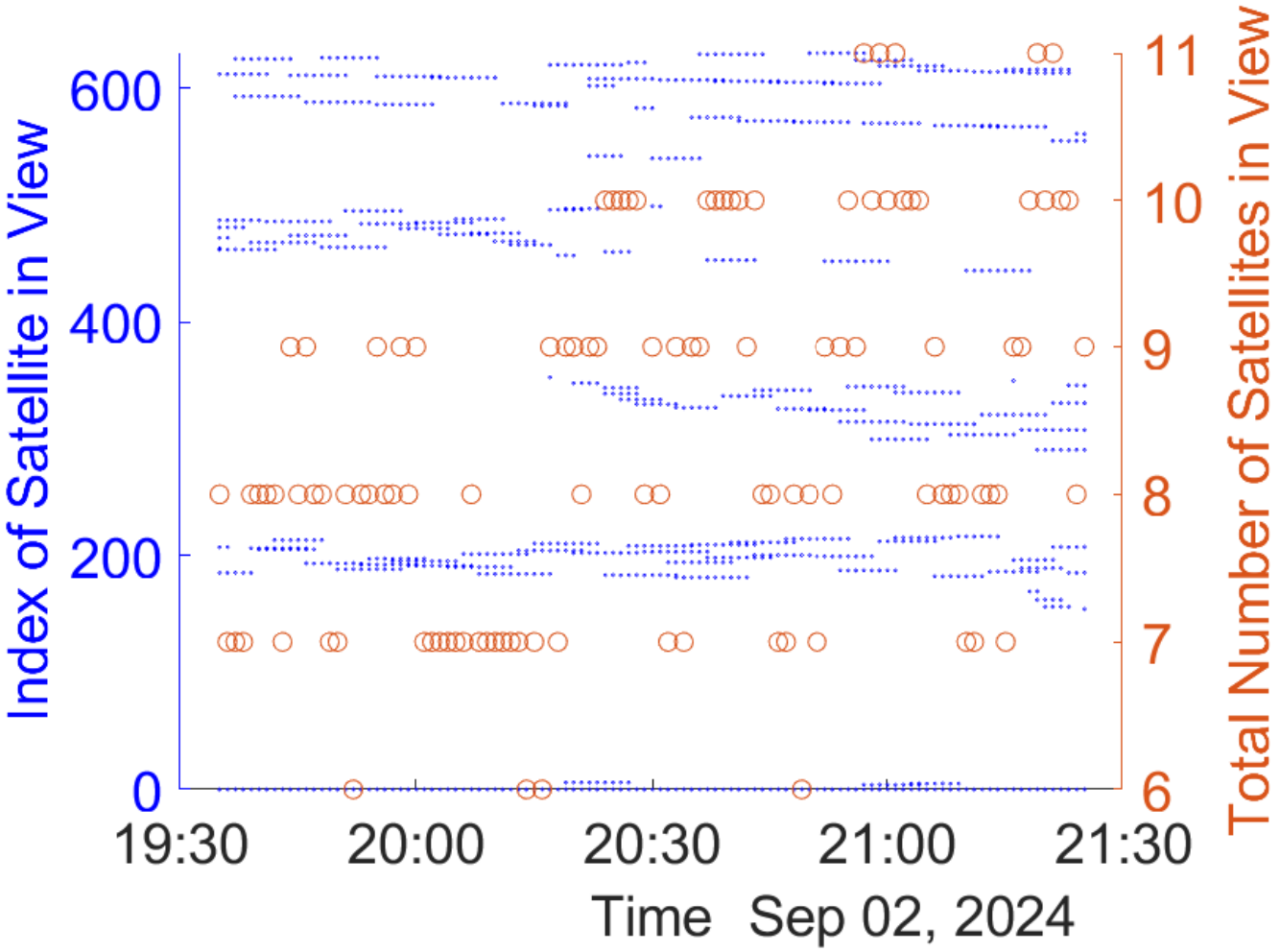

Figure 1: Visibility of OneWeb satellites viewed from Cape Canaveral, FL on Sept 2nd, 2024 from 7:35 to 9:25 pm.

The remainder of this paper develops D-GDOP analysis techniques for time-diverse carrier Doppler shift measurements in two main sections plus a summary and conclusions section. Section II describes the Doppler-only PNT model and associated D-GDOP calculation for a batch filter assuming constant velocity and clock-offset rate. Section III present a preliminary analysis of an improved form of D-GDOP analysis. The improved analysis allows for random variations of acceleration and clock-offset rate that might occur in typical applications. It develops a special Kalman-filter-type analysis in order to define a D-GDOP that

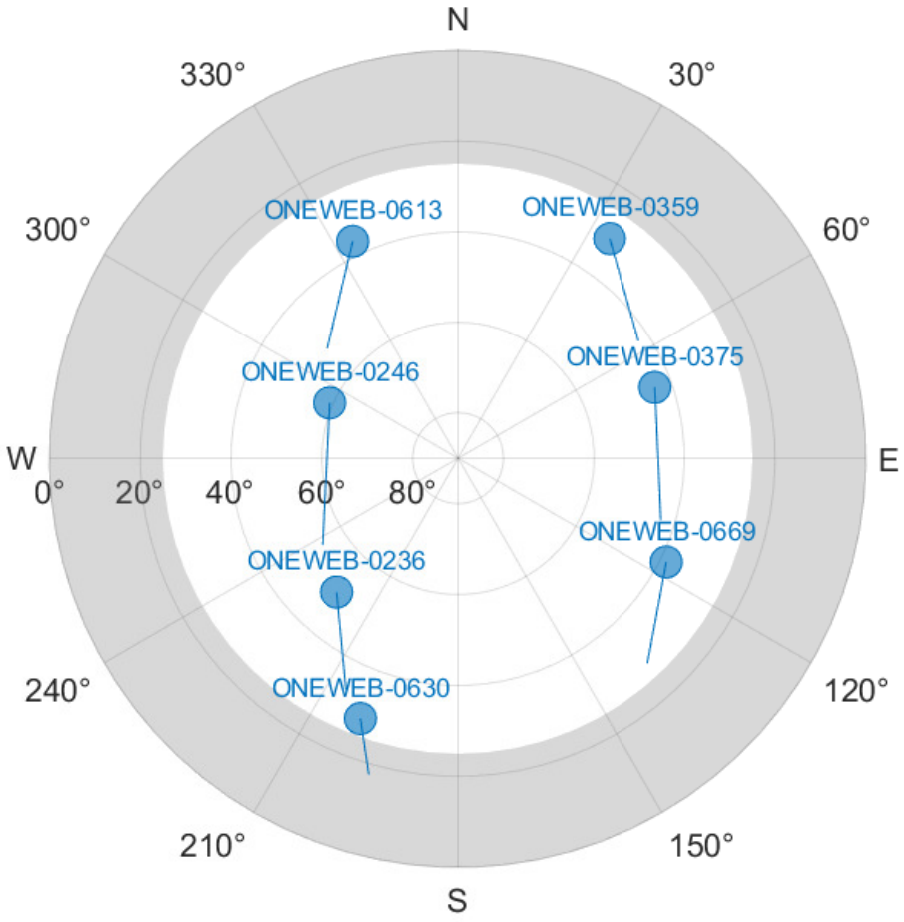

Figure 2: Skyplot showing the path of OneWeb satellites viewed from Cape Canaveral, FL on Sept 2nd, 2024 at 8:46 pm during a period of 100 seconds.

applies to this more realistic situation. This section compares the D-GDOP results and filter estimation error results between the constant-velocity analysis and filter of Section II and the drifting analysis and filter of Section III. Section IV summarizes the work's potential, draws conclusions about it, and discusses possible future work.

II. A DOPPLER-BASED NAVIGATION SOLUTION AND ITS GDOP BASED ON TIME DIVERSITY AND CONSTANT TIME RATES OF CHANGE

In order to use time-diverse Doppler measurements, a navigation solution algorithm must use a model of how its solution relates to the measurements at multiple measurement times. The simplest model that allows for user motion and clock-drift assumes constant time rates of change. That is, the velocity is constant and the clock-offset rate is also constant. Using the notation defined in Psiaki (2021), one can define the position, clock-offset, velocity, and clock-offset rate at time-step k as follows:

$$\vec{r}_k = \vec{r}_M + \vec{v}(t_{Rk} - t_{RM})/(1 + \dot{\delta}_R) \tag{1}$$

$$\delta_{Rk} = \delta_{RM} + \dot{\delta}_R(t_{Rk} - t_{RM})/(1 + \dot{\delta}_R) \tag{2}$$

$$\vec{v}_k = \vec{v} \tag{3}$$

$$\dot{\delta}_{Rk} = \dot{\delta}_R \tag{4}$$

The sample time index k can take on the values $0, 1, 2, ..., M$. The estimated quantities are the terminal position vector $\vec{r}_M$

and terminal clock-offset δ_{RM}, which apply at receiver clock sample time t_{RM}, along with the constant velocity $\vec{v}$ vector and constant clock-offset rate $\dot{\delta}_R$. This set of estimated quantities is the same as the set of estimated quantities in Psiaki (2021) at sample time t_{RM}. That paper would use Doppler shift data at an earlier time, t_{Rk} for some $k < M$, only to estimate the unknowns at that earlier time: $\vec{r}_k$, δ_{Rk}, $\vec{v}_k$, and $\dot{\delta}_{Rk}$, and it would not employ any dynamic model to link these quantities at different sample times.

1. Batch-Filter that uses Data from Multiple Sample Times

The dynamic model in Eqs. (1-4) can be used to modify the point solution batch filter defined in Eq. (14) of Psiaki (2021) to compute estimates of the position, clock-offset, velocity, and clock-offset rate at time-step M based on data from sample instants $k = 0, ..., M$. The modified time-diverse batch filter solves the following non-linear least squares problem:

$$\begin{aligned} &\text{find : } \vec{r}_M, \delta_{RM}, \vec{v}, \text{ and } \dot{\delta}_R \\ &\text{to minimize: } J(\vec{r}_M, \delta_{RM}, \vec{v}, \dot{\delta}_R) = \frac{1}{2} \sum_{k=0}^{M} \sum_{j=1}^{N_k} \left(\frac{\lambda D_k^j + \frac{d\Delta\rho_{ADR}^j}{dt_R}|_{(\vec{r}_k, \delta_{Rk}, \vec{v}, \dot{\delta}_R; t_{Rk})}}{\lambda \sigma_{Dopp}^j} \right) \end{aligned} \tag{5}$$

Note that compared to Eq. (14) of Psiaki (2021) this is now a double summation – over both sample time index k and satellite index j, with N_k being the number of satellites in view at sample time t_{Rk}. In this formula λ is the nominal carrier wavelength of the signal, D_k^j is the measured carrier Doppler shift of the j^{th} satellite at sample time t_{Rk}, $\Delta\rho_{ADR}^j$ is the modeled accumulated delta range from the user receiver to the j^{th} satellite, and σ_{Dopp}^j is the standard deviation of the measurement error in D_k^j. Note that the values of $\vec{r}_k$ and δ_{Rk} that appear on the right-hand side of the cost function formula are computed from $\vec{r}_M$ and δ_{RM}, $\vec{v}$, and $\dot{\delta}_R$ as per the models in Eqs. (1) and (2). To minimize this, use the Gauss-Newton nonlinear least-squares algorithm to find the values of $\vec{r}_M$, δ_{RM}, $\vec{v}$, and $\dot{\delta}_R$ that minimize J.

The 8-satellites-per sample time minimum requirement for batch filter solution existence from Psiaki (2021) changes to the following requirement for this new filter: $N_{totM} = \sum_{k=0}^{M} N_k \geq 8$. This modified requirement allows $N_k < 8$ at any given sample time, which is a major goal of the present paper's developments.

2. Doppler based GDOP for the New Batch Filter

One can develop an updated D-GDOP for this new batch filter by modifying the D-GDOP analysis of Psiaki (2021). Like the D-GDOP analysis of that paper, it is based on a linearized relationship between the Doppler shift measurement errors ΔD_k^j for $j = 1, ..., N_k$ and $k = 0, ..., M$, and the estimation errors $\Delta\vec{r}_M$, $\Delta\delta_{RM}$, $\Delta\vec{v}$, and $\Delta\dot{\delta}_R$. That relationship takes the form:

$$-\begin{bmatrix} \lambda D_0^1 \\ \vdots \\ \lambda D_k^j \\ \vdots \\ \lambda D_M^{N_M} \end{bmatrix} = A \begin{bmatrix} \gamma\Delta\vec{r}_M \\ \eta\Delta\delta_{RM} \\ \Delta\vec{v} \\ c\Delta\dot{\delta}_R \end{bmatrix} \tag{6}$$

where A is an N_{totM}-by-8 non-dimensional coefficient matrix:

$$A = \begin{bmatrix} A_0 \begin{bmatrix} I & F(t_{R0} - t_{RM}) \\ 0 & I \end{bmatrix} \\ A_1 \begin{bmatrix} I & F(t_{R1} - t_{RM}) \\ 0 & I \end{bmatrix} \\ A_2 \begin{bmatrix} I & F(t_{R2} - t_{RM}) \\ 0 & I \end{bmatrix} \\ \vdots \\ A_M \begin{bmatrix} I & F(t_{RM} - t_{RM}) \\ 0 & I \end{bmatrix} \end{bmatrix} \tag{7}$$

where

$$F = \begin{bmatrix} \gamma I_{3\times 3} & 0_{3\times 1} \\ 0_{1x3} & (\eta/c) \end{bmatrix} \tag{8}$$

and

$$A_k = \begin{bmatrix} (\dot{\hat{\rho}}_k^1)^T/\gamma & [(\hat{\rho}_k^1)^T\dot{\vec{v}}^1 + (\dot{\hat{\rho}}_k^1)^T\vec{v}_k^1]/\eta & \hat{\rho}_k^1 & 1 \\ (\dot{\hat{\rho}}_k^2)^T/\gamma & [(\hat{\rho}_k^2)^T\dot{\vec{v}}^2 + (\dot{\hat{\rho}}_k^2)^T\vec{v}_k^2]/\eta & \hat{\rho}_k^2 & 1 \\ \vdots & \vdots & \vdots & \vdots \\ (\dot{\hat{\rho}}_k^{N_k})^T/\gamma & [(\hat{\rho}_k^{N_k})^T\dot{\vec{v}}^{N_k} + (\dot{\hat{\rho}}_k^{N_k})^T\vec{v}_k^{N_k}]/\eta & \hat{\rho}_k^{N_k} & 1 \end{bmatrix}. \tag{9}$$

Note that A_k is the A_{GDOP} matrix defined in Eq. (27) of Psiaki (2021) for a single time sample. The scale factors γ and η are included to give all quantities in the vectors on both sides of the error model in Eq. (8) the same units (m/s). They are functions of a representative semi-major axis of the spacecraft orbits and are defined in Eqs. (24) and (25) of Psiaki (2021). These quantities are, respectively, the maxima of $||\dot{\hat{\rho}}||$ and $|\ddot{\rho}|$ over all satellites, all possible sample times, and all possible user receiver locations. In the preceding equation, $\hat{\rho}_k^j$ is the unit direction vector that points from the j^{th} satellite to the user receiver at sample time t_{Rk}, $\vec{v}_k^j$ is the velocity of the j^{th} satellite at the transmission time associated with sample time t_{Rk}. Note that the time rate of change of the unit direction vector $\hat{\rho}_k^j$ can be shown to be $\dot{\hat{\rho}}_k^j = -\hat{\rho}_k^j \times (\hat{\rho}_k^j \times \frac{\vec{v}-\vec{v}_k^j}{\rho_k^j})$, where ρ_k^j is the scalar distance from the j^{th} satellite to the user receiver at sample time t_{Rk}.

The trailing block matrices involving I and $F(t_{Rk} - t_{RM})$ in Eq. (9) are state transition matrices from the final time to the sample time. Moore et al. (2023) omitted these state transition matrix factors. In effect, it neglected the fact that a non-zero velocity gives rise to a time-varying position and that a non-zero receiver clock offset rate gives rise to a time-varying receiver clock offset.

The new A matrix defined in Eq. (9) can be used to define the D-GDOP for this section's time-diverse Doppler estimation problem. It is:

$$GDOP = \sqrt{Trace[(A^TA)^{-1}]} \tag{10}$$

3. Example Batch Filter Results and D-GDOP Analyses

The batch filter in Eq. (5) and the GDOP calculations in Eqs. (7), (8), and (9) have been applied to example cases. Each example case considers carrier Doppler shift from the OneWeb constellation and uses real-world Two-Line Element (TLE) data from OneWeb that have been downloaded from CelesTrack (2024). The epoch time on the TLEs was for 2 Sept, 2024 and should be accurate for approximately 24hrs. The TLE data are assumed to provide the "truth" satellite locations and are given to both the truth-model simulation that produced simulated data for testing the batch filter and to the batch filter itself. Thus, this study does not consider the effects of orbital ephemeris errors, in keeping with traditional GDOP analyses. The filter and GDOP studies used a 25° elevation mask angle because the planned future OneWeb spot beams will have a limited off-nadir pointing ability that translates into availability only above this mask angle FCC (2013).

A comparison has been made between the D-GDOPs of the original naive analysis – the one that failed to account for the effects of non-zero time rates of change on position and clock offset time histories – and the corrected D-GDOP that has been developed in this section. Figure 3 shows the results for both D-GDOP analyses, the red dots being for the naive analysis and the blue dots being for the corrected analysis. Note how the corrected analysis actually has lower D-GDOP than the original naive analysis. This is true because the correct analysis recognizes that there is additional information about the user velocity and the clock-offset rate that arises from the time dependence of the position and the clock offset. In this way, the previous analysis can be considered a worst case scenario. The fact that all of the naive analysis red dots in Figure 3 lie above the current analysis' blue dots indicate that it errored on the side of pessimism.

Note that Figure 3 is laid out with the horizontal axis time span $t_{RM} - t_{R0}$ increasing from right to to left, which is unconventional. One can think of this time axis as anchoring its right-hand side and the batch filter's terminal estimation time t_{RM}. Points plotted to the left of this final time still tell about the batch filter D-GDOP accuracy metric at the final time t_{RM}, but they are plotted at the start time of the time-diverse data interval that is used to achieve the given level of accuracy at the final time on the right-hand limit of the horizontal axis.

Figure 4 is similar to Figure 3, except for three differences. First, it only plots D-GDOP values from the present section's corrected time-diverse analysis. Second, it plots D-GDOP values for a longer set of batch filter intervals: $t_{RM} - t_{R0}$ extending as far back

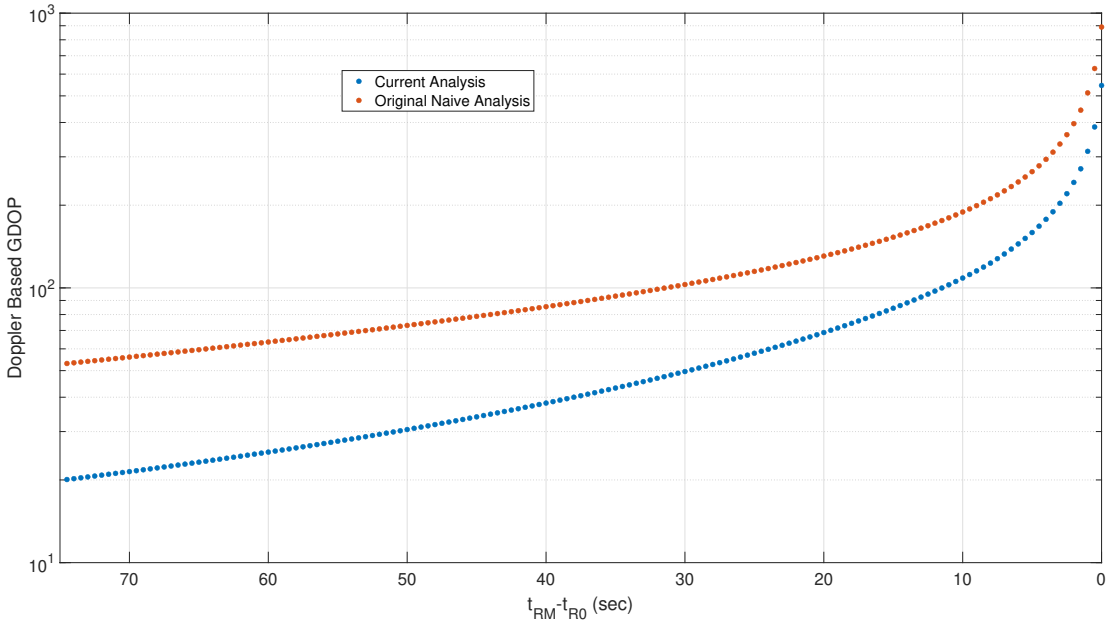

Figure 3: Comparison of D-GDOP metrics as viewed from Cape Canaveral, FL at 8:46 pm on Sept 2nd, 2024.

as 3,000 seconds as opposed to only 75 seconds for Figure 3. Third, it plots the OneWeb constellations' achieved time-diverse D-GDOP for several different locations: Cape Canaveral, FL; Schriever AFB, CO; and Fairbanks, AK. The Fairbanks, AK, case has the lowest D-GDOP as the polar-orbiting OneWeb constellation provides its best coverage in polar regions. The Cape Canaveral, FL, case starts out with a lower D-GDOP than Schriever AFB, CO, for short batch filter time durations due to having a more advantageous geometry at 8:46 pm. All three cases have D-GDOP improving as the batch filter duration $t_{RM} - t_{r0}$ increases, but the Schriever AFB case eventually develops more improvement with increasing batch interval than does the Cape Canaveral case. This is likely due to the to the fact that some satellites traveling South to North appear in the batch filter interval around 7:56 pm. Although D-GDOP continues to decrease as more time-history is considered – as one would expect due to the availability of additional data and the lack of random process noise in the dynamic model of Eqs. (1)-(4) – the marginal improvements of the Cape Canaveral and Fairbanks cases are very small towards the left-hand side of Figure 4. Clearly, there are diminishing returns given by including more historical samples.

Similar to the point-solution batch filter simulations of Psiaki (2021), time-diverse batch filter navigation solutions have been generated for this section's filter in Eq (5). These solutions are generated using simulated truth-model data from 100 Monte Carlo cases. The $\lambda\sigma_{Dopp}$ range-rate-equivalent carrier Doppler shift accuracy level 0.1 m/sec has been used in the simulations, and the sample interval $t_{k+1} = t_k = 0.5$ sec has been used. The true positions for these cases are randomly distributed over the surface of the Earth. The true velocities, clock offsets, and clock offset rates are all assumed to be zero. All simulations initialize the filter's Gauss-Newton iteration with an error of between 143 and 157 meters. The filter was then iterated to the optimum of the problem in Eq. (5) for each case. After doing this for each case, statistics for the resulting errors for the 100 cases were used to generate the filter performance statistics shown in Table 1.

One seemingly counter-intuitive result can be observed in the first two rows of Table 1 for the batch data intervals 0, 10, and 100 seconds: the RMS and/or peak errors are larger than the errors of the Gauss-Newton's method initial guess. In reality, such situations can easily occur for nonlinear batch filters with poor observability. The optimal value can be relatively far from the truth due to the effect of the measurement errors and the poor observability, which will cause the Gauss-Newton iterations to move further away from the truth because the nonlinear least-squares cost function's minimum is further away than the relatively accurate initial guess. If the goal of this simulation study had been to evaluate filter convergence rather than accuracy of the converged solution, then much larger initial filter guess errors would have been used, and this counter-intuitive result would not have been obtained.

The results in Table 1 chiefly illustrate that the accuracy of the batch filter in Eq. (5) improves as the length of the time-diversity window increases. Note how the RMS and peak errors in each line of the table decrease when moving from short durations on the left to long durations on the right. Note that zero duration statistics are included because, in all 100 simulation cases, there

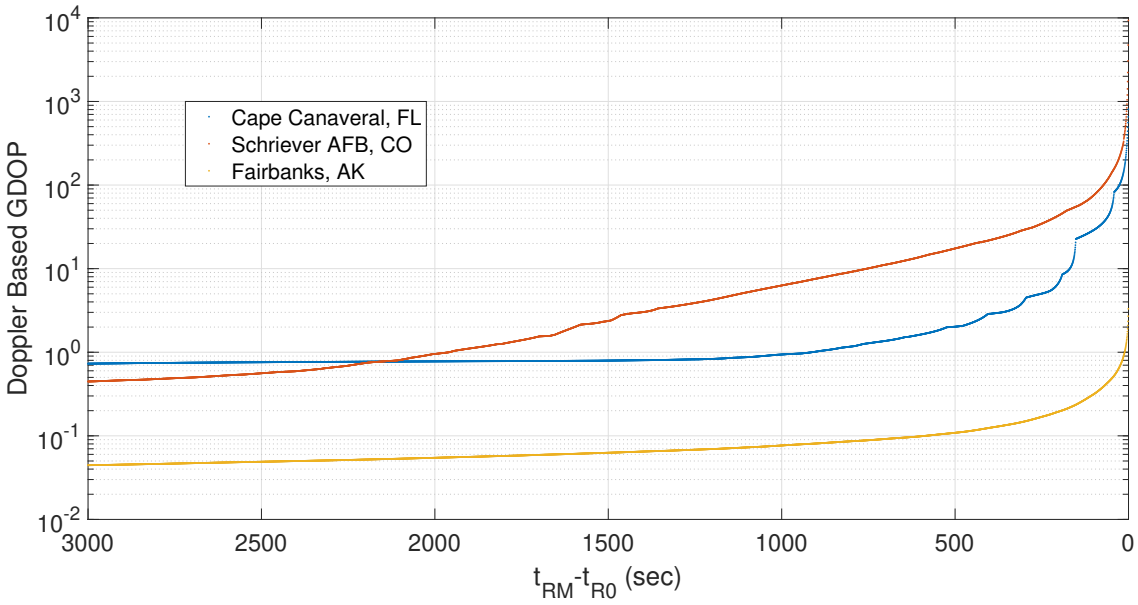

Figure 4: Comparison of D-GDOP as viewed from three locations at 8:46 pm on Sept 2nd, 2024.

Table 1: RMS and Maximum errors over 100 Monte Carlo simulation cases for constant-rates, time-diverse the batch filter model using a variety of data intervals

Error Metric	$t_{RM} - t_{R0}$ (sec) 0	10	100	1000	3000
RMS $\vec{r}$ Error (m)	3,266.6	1,254.2	47.489	4.9114	1.9921
Max $\vec{r}$ Error (m)	22,289	6,480.4	195.81	14.2236	5.9472
RMS $\vec{v}$ Error (m/s)	3.7454	0.9896	0.0581	0.0047	0.0011
Max $\vec{v}$ Error (m/s)	32.654	4.8949	0.2011	0.0132	0.0031
RMS δ_R Error (ms)	555.91	276.21	12.676	1.1795	0.2863
Max $\lvert\delta_R\rvert$ Error (ms)	4,040.8	1,972.1	65.801	5.5439	1.4985
RMS $c\dot{\delta}_R$ (m/s)	4.0976	0.7002	0.0481	0.0050	0.0013
Max $c\lvert\dot{\delta}_R\rvert$ (m/s)	34.761	4.0509	0.1776	0.0234	0.0041

were $N_M >= 8$ satellites available at the batch filter estimation time t_{RM}.

III. MODIFICATION OF FILTER AND D-GDOP TO ACCOUNT FOR RANDOM DRIFT OF VELOCITY AND CLOCK OFFSET RATE

The constant velocity and clock offset rate assumed in the introduced model are unrealistic, especially for long spans of time. The performance of the batch filter could suffer drastically under non-zero acceleration and non-zero clock drift. A more realistic filter and D-GDOP analysis would allow for such drift and model it using stochastic processes. A reasonable approach to the problem of drift modeling is to use techniques associated with a time-varying Kalman filter.

1. Kalman Filter Model

A reasonable approach to the drift problem would be to define a Kalman filter model based on the following 11-element state vector:

$$\mathbf{x}_k = \left[\vec{r}^T(t_{Rk}) \quad c\delta_R(t_{Rk}) \quad \vec{v}^T(t_{Rk}) \quad c\dot{\delta}_R(t_{Rk}) \quad \vec{a}^T(t_{Rk})\right] \tag{11}$$

The elements of this state are the 3 Cartesian components of the ECEF user position vector at sample time t_{Rk}, $\vec{r}(t_{Rk})$, the corresponding range-equivalent receiver clock offset, $c\delta_R(t_{Rk})$, the 3 Cartesian components of the corresponding ECEF user

velocity vector, $\vec{v}(t_{Rk})$, the range-rate-equivalent receiver clock offset rate, $c\dot{\delta}_R(t_{Rk})$, and the 3 Cartesian components of the corresponding ECEF user acceleration vector, $\vec{a}(t_{Rk})$.

The dynamics of this state vector can be defined using the following discrete-time Gauss-Markov linear dynamics model with process noise vector $\mathbf{w}_k$:

$$\mathbf{x}_{k+1} = \begin{bmatrix} I_{3\times3} & 0_{3\times1} & \Delta t I_{3\times3} & 0_{3\times1} & 0.5\Delta t^2 I_{3\times3} \\ 0_{1\times3} & 1 & 0_{1\times3} & \Delta t & 0_{1\times3} \\ 0_{3\times3} & 0_{3\times1} & I_{3\times3} & 0_{3\times1} & \Delta t I_{3\times3} \\ 0_{1\times3} & 0 & 0_{1\times3} & 1 & 0_{1\times3} \\ 0_{3\times3} & 0_{3\times1} & 0_{3\times3} & 0_{3\times1} & e^{-\Delta t/\tau_{acc}} I_{3\times3} \end{bmatrix} \mathbf{x}_k + \\ \begin{bmatrix} 0_{3\times3} & 0_{3\times1} & 0_{3\times1} \\ 0_{1\times3} & c\sqrt{S_f \Delta t + S_g \Delta t^3/3} & 0 \\ 0_{3\times3} & 0_{3\times1} & 0_{3\times1} \\ 0_{1\times3} & \frac{cS_g \Delta t^{3/2}}{2\sqrt{S_f + S_g \Delta t^2/3}} & c\sqrt{\frac{S_g(S_f \Delta t + S_g \Delta t^3/12)}{S_f + S_g \Delta t^2/3}} \\ a_{RMS}\sqrt{1 - e^{-2\Delta t/\tau_{acc}}} I_{3\times3} & 0_{3\times1} & 0_{3\times1} \end{bmatrix} \mathbf{w}_k \tag{12}$$

where τ_{acc} is the time constant of the first-order Gauss-Markov acceleration, a_{RMS} is its steady-state acceleration standard deviation, Δt is the sample interval so that $\Delta t = t_{k+1} - t_k$, S_f and S_g are the power spectral densities of, respectively, the clock-offset random walk component and the clock-offset rate random-walk component. S_f has units of seconds, and S_g has units of 1/sec. The two clock drift modeling parameters can be computed from the minimum root Allan variance and the delay at which that minimum occurs, per Brown and Hwang (1997). Note that the 5-by-1 process noise vector $\mathbf{w}_k$ is a Gaussian random white noise sequence with a mean of zero and a covariance equal to the identity matrix.

The Kalman filter measurement model is the model given in Eq. (1) of Psiaki (2021). Its nonlinearities make this Kalman filter model nonlinear despite the fact that the dynamics model is linear. For purposes of GDOP analysis, a linearized version of the measurement model can be used. It takes the form:

$$\Delta \boldsymbol{y}_k = A_k \begin{bmatrix} \gamma I_{3\times3} & 0_{3\times1} & 0_{3\times3} & 0_{3\times1} & 0_{3\times3} \\ 0_{1\times3} & (\eta/c) & 0_{1\times3} & 0 & 0_{1\times3} \\ 0_{3\times3} & 0_{3\times1} & I_{3\times3} & 0_{3\times1} & 0_{3\times3} \\ 0_{1\times3} & 0 & 0_{1\times3} & 1 & 0_{1\times3} \end{bmatrix} \Delta \boldsymbol{x}_k + \boldsymbol{\nu}_k \tag{13}$$

where the N_k-by-8 matrix A_k has been defined in Eq. (9), $\Delta \boldsymbol{y}_k$ is the N_k-by-1 vector of range-rate-equivalent carrier Doppler shift perturbations from the nominal estimate value for this quantity, $\Delta \boldsymbol{x}_k$ is the perturbation of the state from its nominal estimate, and $\boldsymbol{\nu}_k$ is the random measurement noise.

2. Generalization of D-GDOP to Kalman Filter Model to Account for Velocity and Clock Drift

The definition of the non-dimensional D-GDOP accuracy metric for a time-varying Kalman filter is not immediately obvious. A reasonable definition can be developed if one starts by initializing a Kalman filter based on the previous subsection's model a very long time before the time at which one wants to calculate its D-GDOP. Suppose that this D-GDOP calculation time is t_{Rk}. Suppose, also, that the 11-by-11 Kalman filter estimation error covariance matrix at this time is P_{xxk} for a filter that has been initialized a long time prior to time t_{Rk}. One can non-dimensionalize the upper left 8-by-8 block of this covariance matrix by performing the following calculation:

$$P_{ndk} = \frac{1}{(\lambda \sigma_{Dopp})^2} \begin{bmatrix} \gamma I_{3\times3} & 0_{3\times1} & 0_{3\times4} & 0_{3\times3} \\ 0_{1\times3} & \eta/c & 0_{1\times4} & 0_{1\times3} \\ 0_{4\times3} & 0_{4\times1} & I_{4\times4} & 0_{4\times3} \end{bmatrix} P_{xxk} \begin{bmatrix} \gamma I_{3\times3} & 0_{3\times1} & 0_{3\times4} & 0_{3\times3} \\ 0_{1\times3} & \eta/c & 0_{1\times4} & 0_{1\times3} \\ 0_{4\times3} & 0_{4\times1} & I_{4\times4} & 0_{4\times3} \end{bmatrix}^T \tag{14}$$

One can use this 8-by-8 matrix in order to define a sensible D-GDOP at time-step k as follows:

$$GDOP_k = \sqrt{\text{trace}(P_{ndk})} \tag{15}$$

3. Example Kalman-Filter-Based D-GDOP and Accuracy Results

In order to understand the benefit of this Kalman-filter-based analysis, it is helpful to compare the batch and Kalman filters under non-zero acceleration and non-zero clock drift. This has been been done by computing the D-GDOP values for both

filters over a range of assumed data spans and by using both filters to process truth-model simulation data. The truth model simulation uses velocity and clock drift models consistent with Eq. (12), except that there is a weak outer feedback loop from position, velocity and acceleration in the simulation that keeps the position from wandering more than about 5,000 meters from the nominal simulated ECEF position. The simulation uses $a_{acc} = (9.81/4)m/sec^2$, i.e., a quarter g of acceleration steady-state standard deviation, along with S_f and S_g clock drift parameters that yield a minimum root-Allan variance of 3.2×10^{-9} at a delay of 100 seconds. Note that the batch filter still assumes a constant velocity and a constant clock-offset rate. Figure 5 shows the D-GDOP of the two filters at Cape Canaveral, FL, for a variety of durations. Recall that the horizontal axis duration for the batch filter defines the duration of its data batch, $t_{RM} - t_{R0}$. For the Kalman filter, the horizontal axis defines the amount by which the filter initialization time precedes the GDOP calculation time t_{Rk}. Given that the Kalman filter assumes infinite a priori covariance at its initialization time, which is possible by virtue of its Square-Root Information Filter Initialization, the two filters are comparable. They base their estimates at the end time of their respective data spans solely on the same set of carrier Doppler shift measurements taken over that span. The batch filter has lower D-GDOP than the Kalman filter which means that the batch filter thinks that it achieves more accuracy than the Kalman filter. This would be true if its constant-velocity and constant-clock-offset-rate assumptions were true. The fact that the actual truth-model data does not fit its assumptions, however, causes its assessment of its own accuracy to be wildly optimistic. At 100 sec data batch duration, the Kalman filter achieves a position error of only 3.05m while the batch filter exhibits an error of 21.6km. At a 1500 sec data batch duration, the Kalman filter achieves a position error of 2.77m while the batch filter has an error 15.6km. The batch filter performs extremely poorly because the assumptions it holds (constant velocity and clock-offset rate) are not true. This also causes the batch filter to severely underestimate its D-GDOP – it thinks it will perform much better than it does. The Kalman filter, on the other hand, is much more accuraate, and its corresponding D-GDOP is consistent with its accuracy. It sensibly recognizes that there is a practical limit to the duration of past data that can help to for its estimate of the state at any given sample time t_{Rk}. This sensible property of the Kalman filter is evidenced by the fairly rapid convergence of its calculated D-GDOP to a constant value as the data interval increases from its initialization to its t_{Rk} output time.

These initial results for the Kalman-filter-based D-GDOP analysis are encouraging. Note, however, that further testing will be necessary under more varied conditions in order to better assess its applicability as a practical accuracy metric for time-diverse carrier-Doppler-based navigation.

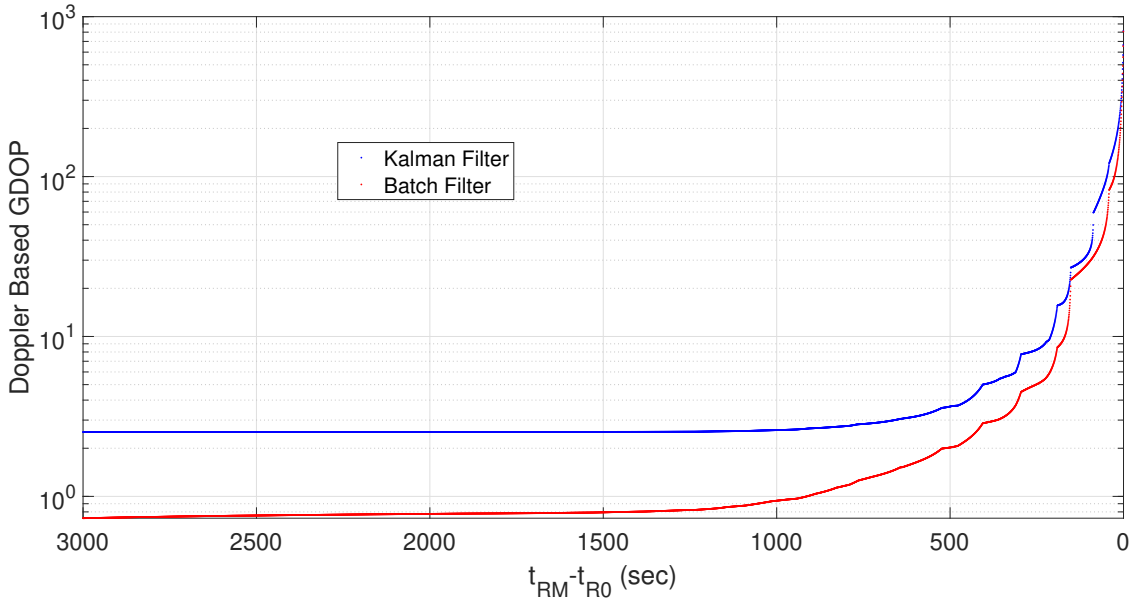

Figure 5: Comparison of D-GDOP for the Kalman filter and batch filter models. Viewed from Cape Canaveral, FL at 8:46 pm on Sept 2nd, 2024.

IV. SUMMARY AND CONCLUSIONS

Doppler-only positioning from signals of opportunity from LEO constellations has been considered in the case where one cannot guarantee that signals from eight or more satellites are simultaneously available. The concept of time-diverse signals has been explored where by a multiplicity of samples from one or more satellites can compensate for the inability to see eight signals

simultaneously. Two filters have been proposed and analyzed to process such data. One is a batch filter that assumes constant receiver velocity and constant receiver clock offset rate. The other is a Kalman filter that models non-zero acceleration and clock offset rate drift using stochastic models. In addition to filters, this paper has developed generalizations of GDOP to provide an accuracy metric for each of the two filters.

The batch filter performs well when its constant velocity and constant clock drift rate assumptions are valid. These assumptions, however, are unrealistic especially for long observation intervals, and long observation intervals may be needed in order to achieve a low enough GDOP metric for the batch filter. When tested for random non-zero acceleration and clock drift, the batch filter D-GDOP underestimates and has very high position error ($>$10km).The Kalman filter shows good accuracy in the face of non-zero stochastic acceleration and clock offset rate drift, achieving accuracies on the order of standard GPS pseudorange-based solutions. Furthermore, its D-GDOP values give reasonable predictions of its potential accuracy. Further testing under of the Kalman filter and its D-GDOP metric under different conditions is recommended as important future work..

V. ACKNOWLEDGEMENTS

This work has been supported in part by the CARNATIONS contract from the U.S. Department of Transportation under the University Transportation Centers Program (20.701). Ms. Karen Van Dyke is the contract monitor.

REFERENCES

Brown, R. G. and Hwang, P. Y. C. (1997). *Introduction to Random Signal Analysis & Kalman Filtering: With Matlab Exercises Solutions*. J. Wiley & Sons, New York, 3rd edition.

CelesTrack (2024). Supplemental GP element sets. https://celestrak.org/NORAD/elements/supplemental/. Accessed 2 Sept, 2024.

Dovis, F. (2015). *GNSS Interference Threats and Countermeasures*. Artech House.

FCC (2013). OneWeb non-geostationary satellite system: Attachment: A.

FCC (2018). SpaceX non-geostationary satellite system: Attachment A.

Furchtgott-Roth, D. (2022). America needs GPS backup. In *Forbes Magazine*.

Kassas, Z., Kozhaya, S., Saroufim, J., H., K., and S., H. (2023). A look at the stars: navigation with multi-constellation LEO satellite signals of opportunity. In *Inside GNSS Magazine*, volume 18, pages 38–47.

McLemore, B. and Psiaki, M. L. (2021). GDOP of navigation using pseudorange and doppler shift from a LEO constellation. In *Proceedings of the 34th International Technical Meeting of the Satellite Division of The Institute of Navigation (ION GNSS+ 2021)*, pages 2783–2803.

Moore, M. O., Headley, W. C., and Buehrer, R. M. (2023). Time-diverse doppler-only LEO PNT. In *MILCOM 2023 - 2023 IEEE Military Communications Conference (MILCOM)*, pages 950–956, Boston, MA.

Psiaki, M. L. (2021). Navigation using carrier doppler shift from a LEO constellation: TRANSIT on steroids. *NAVIGATION: Journal of the Institute of Navigation*, 68(3):621–641.